

Nonlinear elastic model for faceting of vesicles with soft grain boundaries

Rastko Sknepnek* and Monica Olvera de la Cruz†

Department of Materials Science and Engineering, Northwestern University, Evanston, Illinois 60208

We use an elastic model to explore faceting of solid-wall vesicles with elastic heterogeneities. We show that faceting occurs in regions where the vesicle wall is softer, such as areas of reduced wall thicknesses or concentrated in crystalline defects. The elastic heterogeneities are modeled as a second component with reduced elastic parameters. Using simulated annealing Monte Carlo simulations we obtain the vesicle shape by optimizing the distributions of facets and boundaries. Our model allows us to reduce the effects of the residual stress generated by crystalline defects, and reveals a robust faceting mechanism into polyhedra other than the icosahedron.

Nature uses various vesicular structures to compartmentalize and differentiate matter in order to achieve a desired set of functions. Depending on their origin and function, vesicles can take a wide variety of shapes and sizes with very different physical and chemical properties. A prototypical example of a faceted structure is the capsid of large viruses, for which an icosahedral shape was elegantly described by Caspar and Klug [1]. Next to these regular polyhedra, bacterial micro-components such as carboxysomes [2] (found in cyanobacteria [3], for example), are known to take on irregular faceted shapes. X-ray diffraction of small ($\sim 30\text{nm}$ diameter) single-walled DPPC vesicles found [4] that below the thermal transition they facet into polyhedra. Thick-wall nested fullerenes are also known to sometimes take faceted shapes [5]. Faceted shapes were recently observed [6] by coassembling oppositely charged amphiphiles. It has been argued that under the right conditions electrostatic correlations can lead to faceting [7] or even a complete collapse of the structure [8].

The existence of facets separated by sharp edges that have been observed in experiments can be understood in terms of the vesicle wall being, at least in part, solid [4] or as a result of excess amphiphiles exhibiting spontaneous curvature being present in sufficient quantity [9, 10]. Molecules within a solid wall have fixed connectivity and the vesicle can sustain shear, bending, and stretching deformations. The microscopic structure and properties of the ordered phase is intimately related to the vesicle topology. Very interesting phenomena occur if the local molecular order favored by interactions is not compatible with the global topology and thus cannot be realized simultaneously throughout the whole surface [11]. For example, the preferred planar ordering of identical particles interacting with a spherically symmetric pair potential is a hexagonal lattice, where each site has exactly six equidistant nearest neighbors. In other words, it is possible to tile a plane with equilateral triangles. However, this is not the case for a sphere, and topological defects (i.e., sites with coordination $z \neq 6$) are necessarily present. For a triangular tessellation of a sphere, Euler's theorem ensures that there are at least 12 sites that are five-coordinated [11]. These disclination defects repel each other and take a conformation that maximizes their mutual separation, thus positioning themselves at the vertices of an inscribed icosahedron.

The stretching energy of a five-fold disclination on a plate of radius r is $\propto r^2$ [12]. If the plate is allowed to buckle out of plane it can reduce the stretching energy at the expense of a bending penalty that is $\propto \log r$ [12] and form a cone with the apex centered at the defect. On a sphere these two energies follow the same scaling laws, albeit with different prefactors [13]. If the sphere is sufficiently large it can lower its energy by buckling into an icosahedron via a similar conical deformation seeded at the twelve defects [14]. Recently we have shown that if a vesicle is assembled of multiple molecular species with different elastic properties, depending on the relative ratio and the line tension of the components, it can take a number of regular and irregular polyhedral [15] or Janus-like shapes [16].

These results suggest that a more general buckling mechanism is possible when the vesicles are not elastically homogeneous. However, in a previous work [15] we studied two-component elastic shells with the twelve five-fold defects fixed to the corners of an inscribed icosahedron. Here we show that faceting occurs even if such restrictions are lifted. In this paper we introduce a nonlinear elastic model to study faceting of a vesicle with solid domains connected with soft boundaries. We argue that material heterogeneities, such as local variations in the wall thickness or due to defects in the crystalline order, can lead to local softening of the vesicle wall and provide a pathway for lowering the energy. In order to satisfy both, the preferred local flatness of the solid domains and the curved global geometry the curvature is focused along the softer domain boundaries, which leads to faceting of the entire vesicle.

We assume that the vesicle wall is thin compared to its radius, R , and can be represented as its two-dimensional midsurface. Such an approximation is indeed justified as the vesicle wall is typically a few nanometers thick compared to the radius that ranges from tens of nanometers to microns. The midsurface can be parametrized with two parameters s^1 and s^2 , as a locus of points $\mathbf{r} = \mathbf{r}(s^1, s^2)$. The metric tensor is defined as $g_{\alpha\beta} = \partial_\alpha \mathbf{r} \cdot \partial_\beta \mathbf{r}$, where $\alpha, \beta = 1, 2$. The second fundamental form, related to the surface curvature, is given by $b_{\alpha\beta} = \partial_\alpha \mathbf{r} \cdot \mathbf{n}$, with \mathbf{n} being the unit normal. The elastic energy of the midsurface can be written as [17]

$$E = \int dA \mathcal{A}^{\alpha\beta\gamma\delta} \left(\frac{h}{2} u_{\alpha\beta} u_{\gamma\delta} + \frac{h^3}{24} b_{\alpha\beta} b_{\gamma\delta} \right), \quad (1)$$

where $u_{\alpha\beta} = \frac{1}{2} (g_{\alpha\beta} - \bar{g}_{\alpha\beta})$ is the strain tensor, $\bar{g}_{\alpha\beta}$ is a reference metric, $dA = \sqrt{|g|} ds^1 ds^2$ is the area element, $|\cdot|$ is the

* sknepnek@gmail.com

† m-olvera@northwestern.edu

determinant, $h \ll R$ is the vesicle thickness and the summation over pairs of repeated indices is assumed. Compared to a recent study [18], here we follow Koiter's arguments [19] and retain only terms consistent with the Kirchhoff-Love assumptions [20] of a negligible normal stress. The rank-four elastic tensor $\mathcal{A}^{\alpha\beta\gamma\delta}$ is determined by the material properties. If the material is isotropic $\mathcal{A}^{\alpha\beta\gamma\delta}$ depends only the Young's modulus Y and Poisson's ratio ν , and $\mathcal{A}^{\alpha\beta\gamma\delta} = \frac{Y}{1+\nu} \left(\frac{\nu}{1-\nu} \bar{g}^{\alpha\beta} \bar{g}^{\gamma\delta} + \bar{g}^{\alpha\gamma} \bar{g}^{\beta\delta} \right)$, with $\bar{g}^{\alpha\gamma} \bar{g}_{\gamma\beta} = \delta_{\beta}^{\alpha}$ and δ_{β}^{α} being the Kronecker delta symbol.

The first term in Eq. (1) represents energy associated with stretching deformations while the second term accounts for bending. For an isotropic material the stretching and bending energies simplify to

$$E_s = \frac{h}{2} \int dA \frac{Y}{1+\nu} \left(\frac{\nu}{1-\nu} u_{\alpha}^{\alpha} u_{\beta}^{\beta} + u_{\alpha}^{\beta} u_{\beta}^{\alpha} \right), \quad (2)$$

$$E_b = \frac{h^3}{24} \int dA \frac{Y}{1+\nu} \left(\frac{\nu}{1-\nu} b_{\alpha}^{\alpha} b_{\beta}^{\beta} + b_{\alpha}^{\beta} b_{\beta}^{\alpha} \right), \quad (3)$$

with $u_{\alpha}^{\beta} = \bar{g}^{\beta\gamma} u_{\alpha\gamma}$ and $b_{\alpha}^{\beta} = \bar{g}^{\beta\gamma} b_{\alpha\gamma}$. With the mean curvature $H \equiv \frac{1}{2} b_{\alpha}^{\alpha}$ and the Gaussian curvature $K \equiv \det(b_{\alpha}^{\beta})$, the bending energy can be rewritten as $E_b = \int dA \kappa (2H^2 - (1-\nu)K)$, where $\kappa = \frac{h^3}{12} \frac{Y}{(1-\nu^2)}$ is the bending rigidity. The prefactor of the Gaussian curvature term is negative and proportional to κ , thus suppressing saddle-like ($K < 0$) conformations. For a homogeneous vesicle with fixed topology the Gauss-Bonnet theorem ensures that $\int dA K = \text{const.}$ and the Gaussian curvature term can be omitted. However, for a multicomponent vesicle, as is the case here, this term must be retained.

Variation of Eq. (1) with respect to $u_{\alpha\beta}$ and $b_{\alpha\beta}$ leads to a set of nonlinear partial differential equations for the mechanical equilibrium [18, 20]. Instead of directly solving those equations, which is a formidable task even in simple geometries, we opt for a numerical minimization of the energy, Eq. (1), via Monte Carlo (MC) simulations. The vesicle is represented as a discrete triangular mesh with two types of triangles, *soft* and *hard*. From Eqs. (2) and (3) it is evident that for a fixed Young's modulus Y and Poisson's ratio ν both bending and stretching moduli depend only on the vesicle wall thickness, h . Therefore, for simplicity, we assume that the elastic properties of a component are determined by its thickness, with the soft component being thinner. This allows us to explore the phase behavior as a function of only two parameters, relative thickness $\eta = \frac{h_{\text{hard}}}{h_{\text{soft}}}$ and the fraction f of the soft component. We keep in mind, however, that in the experimental systems the elastic properties are likely to be determined by the local organization of the molecules rather than by the thickness variations. The discrete stretching energy is [21] $E_s^{\text{dis.}} = \sum_T \frac{Y h A_T}{8(1+\nu)} \left(\frac{\nu}{1-\nu} (\text{Tr} \hat{F})^2 + \text{Tr} \hat{F}^2 \right)$,

where $\hat{F} = \hat{g}^{-1} \hat{g} - \hat{I}$ is the Cauchy-Green strain tensor, A_T is triangle area and the sum is carried out over all triangles. Matrices \hat{g} and \hat{g} are the discrete versions of the reference and actual metric tensors, respectively, whose elements are the scalar products of the two vectors spanning each triangle

before and after the deformation. The bending energy of the discrete mesh is [12] $\tilde{\kappa} \sum_{T_i, T_j} (1 - \mathbf{n}_i \cdot \mathbf{n}_j)$ with $\tilde{\kappa} = \frac{2}{\sqrt{3}} \kappa$ [12, 22] and the sum runs over all pairs of the nearest neighbor triangles. We point out that the last expression is actually a discrete version of the continuum energy $\int dA \kappa (2H^2 - K)$ [12]. Therefore, we also need a discrete expression for the $\kappa \nu \int dA K$ term. Gaussian curvature at a vertex i is [23] $K_i \equiv \int_{A_i} K dA_i = 2\pi - \sum_T \phi_T$, where ϕ_T is the angle of the adjacent triangle T at i and $A_i = \frac{1}{3} \sum_T A_T$ is the associated vertex area. Finally, [23] $\kappa \nu \int dA K \rightarrow \kappa \nu \sum_T \frac{A_T}{3} \sum_i \frac{K_i}{A_i}$, where the i -sum runs over the three vertices of triangle T .

The surface mesh was constructed by building a triangulation with N_v vertices randomly (but evenly) distributed on a sphere. The mesh with N_t triangles was generated with the 3D Surface Mesh Generation package in the CGAL library [24]. In order to ensure that the results are insensitive to the discretization details we have performed independent runs starting from different initial configurations with 2×10^3 to 5×10^3 vertices and 4×10^3 to 10^4 triangles. Furthermore, we have validated our results using regular triangulations of comparable sizes constructed according to the prescription introduced by Caspar and Klug [1]. $N_t^{\text{soft}} = f N_t$, where $f = 0.01 \dots 0.4$ is the fraction of randomly chosen triangles were designated as soft. For a given random mesh we have explored at least two different initial random distributions of the soft triangles, removing a possible bias caused by a particular choice of the initial distribution of the components. The reference metric \hat{g} is an input parameter in our model and was chosen to be that of the initial triangulation, which removes the instability toward buckling into an icosahedron discussed in Ref. [14]. However, some residual stress is still present as the stretching energy is minimized in the spherical configuration while the bending energy favors flat faces. In order for the bending energy to win, the vesicle wall has to be sufficiently thick. From Eqs. (2) and (3) bending and stretching energies are comparable at $h \approx a$, where a is the unit length set by the average edge length of a triangle. Our model implicitly assumes that each triangle contains a sufficient number of microscopic degrees of freedom such that the molecular details are of no importance. In an typical amphiphilic system $a \approx 5\text{nm}$ sets the length scale down to which the continuum description is applicable. We set $h_{\text{hard}} = a$ ($a \ll R$ and the thin plate approximation is valid) and note that in the $h_{\text{hard}} \rightarrow 0$ limit the vesicle would remain spherical regardless of the thickness ratio $\eta = \frac{h_{\text{hard}}}{h_{\text{soft}}}$. Therefore, in our model a finite thickness is essential for faceting to occur. Setting \hat{g} to be flat leads to interesting effects which will be addressed elsewhere. In order to find the optimal vesicle shape and the distribution of components simulated annealing MC simulations were performed. A MC step consisted of two moves: (i) A random displacement of a vertex was attempted, followed by (ii) an attempted swap of the component types of a randomly chosen pair of triangles. Both moves were accepted according to the Metropolis algorithm. The system was heated up and cooled down using a linear cooling protocol followed by three consecutive exponential cooling runs. For each run, the configuration found to have the lowest energy was recorded.

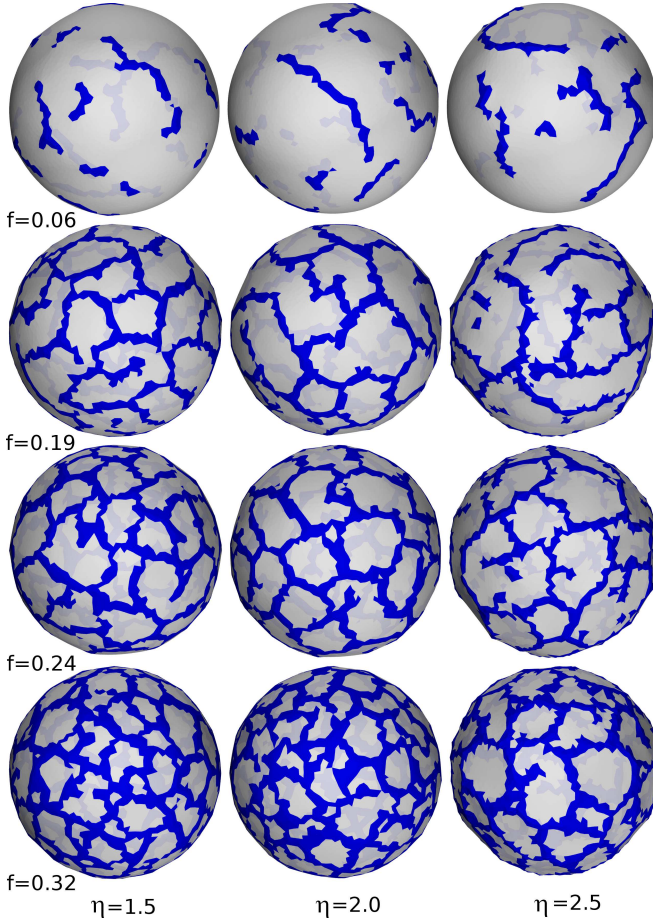


Figure 1. (color online) Snapshots of typical vesicle shapes as a function of the thickness ratio $\eta = h_{\text{hard}}/h_{\text{soft}} = 1.5, 2.0, 2.5$ and the fraction of the soft component $f = 0.06, 0.19, 0.24$ and 0.32 . The soft component is shown in blue (dark) while the hard component is white (light) and slightly transparent. For clarity, width of the soft-component region has been enhanced.

A typical run consisted of 4×10^5 MC sweeps. Note that the triangle type swap move is just a tool to optimize the component distribution and does not correspond to the actual redistribution of the molecules that occurs during the vesicle assembly. The actual kinetics of the self-assembly process is complex and beyond the scope of this work.

We set Poisson's to $\nu = \frac{1}{3}$, measure energies in units of Yh/a^2 and measure mean and Gaussian curvatures in units of $1/a$ and $1/a^2$, respectively. Note that the energy landscape is complex and the simulated annealing is unlikely to find actual ground state configurations. However, all obtained structures are qualitatively reproducible and are thus referred to as *typical*. In Fig. 1 we present snapshots of typical vesicle shapes for a range of fractions f of the soft component and relative thicknesses, $\eta = \frac{h_{\text{hard}}}{h_{\text{soft}}}$. For $f \lesssim 0.1$, the soft component forms elongated, mutually disconnected ridges on the vesicle surface. The vesicle remains nearly spherical with slight distortions near the ridges. As f increases to ≈ 0.2 , ridges begin to merge and facets develop. The onset of faceting is not sharp

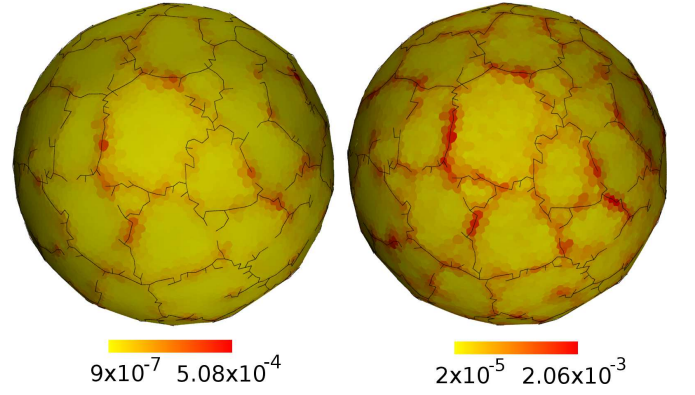


Figure 2. (color online) Distribution of stretching E_s (left) and bending E_b (right) energies for $\eta = 2.0$ and $f = 0.25$. Black lines indicate the soft boundaries between facets. For visualization purposes, a lattice dual to the actual triangulation is shown.

and appears to be sensitive to η . If the amount of the soft component is further increased the number of facets increases and they become smaller in size. We speculate that for $f \gtrsim 0.5$ this would no longer be the case and the soft component would form islands; however, we have not explored this regime as it is not applicable to the experimental systems of present interest. The hard-component facets are, however, not perfectly flat and their curvature depends on η . For $\eta \lesssim 1.5$ the vesicle appears almost spherical, while for $\eta \gtrsim 2.5$ its shape is clearly polyhedral.

In Fig. 2 we show the distribution of the stretching and bending energies on the vesicle surface for $\eta = 2.0$ and $f = 0.25$. As expected, the stretching energy is highest along the boundaries where the material is soft. Note that the stretching energy is particularly large near the kinks in the soft boundary suggesting that such structures are probably not energetically preferred. Relaxing these kinks requires a coherent global redistribution of the components that is very hard to achieve in most numerical optimization schemes.

In Fig. 3 we show the distribution of the mean curvature for a vesicle with $f = 0.25$ and $\eta = 2.0$ with two distinct peaks. The sharper peak at low H corresponds to the facets, while the weaker broader peak at a larger H represents the curvature at boundaries. A projection plot of H clearly shows that the high curvature is condensed along lines. Distribution of the Gaussian curvature is shown in Fig. 4 with a sharp peak at zero. Although $K = 0$ on the facets, $H > 0$ indicating that the facets are not flat but locally cylindrical. Gaussian curvature is localized along the soft grain boundaries as can be seen in the projection plot in the inset in Fig. 4. We note that a number of vertices have $K < 0$. Such regions locally resemble saddles and are located along the soft-component ridges. A detailed analysis of this effect would require a finer mesh and a more accurate minimization technique than used here.

We have implemented a general non-linear elastic model to analyze faceting of solid-wall vesicles with soft domain boundaries into polyhedra other than icosahedra. By choosing a suitable reference metric state, we have removed the in-

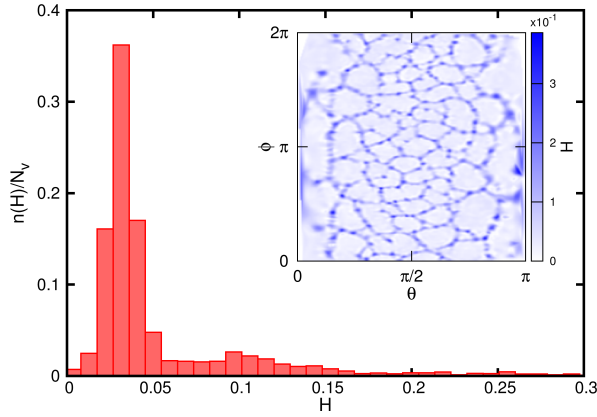


Figure 3. (color online) Distribution of the mean curvature, H , for $f = 0.25$ and $\eta = 2.0$ with two peaks corresponding to the hard facets (lower H) and soft boundaries (higher H). *Inset*: Projection, $\phi\theta$ -plot of H . Darker colors indicate high curvature regions. Blurry distortions near the plot edges are an artifact of the interpolation method.

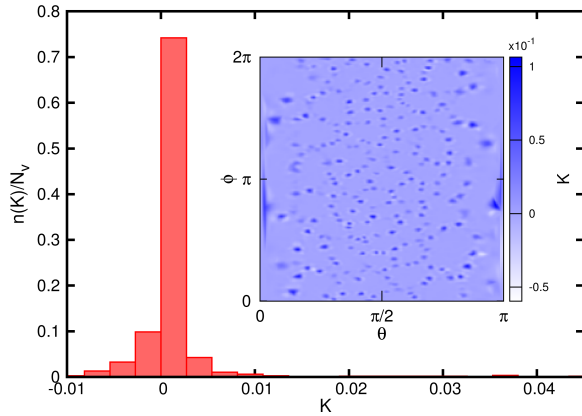


Figure 4. (color online) Distribution of the Gaussian curvature, K , for $f = 0.25$ and $\eta = 2.0$. *Inset*: Projection, $\phi\theta$ -plot of K . Darker colors indicate high Gaussian curvature regions. Blurry distortions near the plot edges are an artifact of the interpolation method.

stability toward buckling into the icosahedron seeded at the twelve five-fold defects [14]. While topological defects are still present as required by the spherical topology their effects are treated implicitly by assuming that they collect at the boundary between facets making the vesicle wall locally soft. Consequently the long-range effect of the stress produced by the defects are substantially suppressed resulting in faceting into irregular polyhedra. We believe that our model qualitatively explains the faceting observed in small DPPC vesicles [4] and vesicles coassembled by oppositely charged amphiphiles [6]. We conclude by noting that other nonspherical shapes have also been observed in multicomponent liquid vesicles [23] and in vesicles assembled of smectic polymer molecules [25, 26].

We thank C. Funkhouser, V. Jadhao, C. Thomas, and G. Vernizzi for numerous comment on the manuscript. Numerical simulations were performed using the Northwestern High Performance Computing Cluster - Quest. This work was supported by the US Department of Energy Award DEFG02-08ER46539 and by the US Air Force Office of Research NSEFF Award.

[1] D. L. D. Caspar and A. Klug, Cold Spring Harbor Symposia on Quantitative Biology **27**, 1 (1962).
[2] C. V. Iancu, D. M. Morris, Z. Dou, S. Heinhorst, G. C. Cannon, and G. J. Jensen, Journal Of Molecular Biology **396**, 105 (2010).
[3] T. Yeates, C. Kerfeld, S. Heinhorst, G. Cannon, and J. Shively, Nature Reviews Microbiology **6**, 681 (2008).
[4] A. Blaurock and R. Gamble, Journal of Membrane Biology **50**, 187 (1979).
[5] D. Srolovitz, S. Safran, M. Homyonfer, and R. Tenne, Phys.

Rev. Lett. **74**, 1779 (1995).
[6] M. A. Greenfield, L. C. Palmer, G. Vernizzi, M. Olvera de la Cruz, and S. I. Stupp, Journal of the American Chemical Society **131**, 12030 (2009).
[7] G. Vernizzi and M. Olvera de la Cruz, Proceedings of the National Academy of Sciences of the United States of America **104**, 18382 (2007).
[8] R. Sknepnek, G. Vernizzi, and M. Olvera de la Cruz, Physical Review Letters **106**, 215504 (2011).
[9] C. A. Haselwandter and R. Phillips, Phys. Rev. Lett. **105**,

- 228101 (2010).
- [10] C. A. Haselwandter and R. Phillips, Phys. Rev. E **83**, 061901 (2011).
 - [11] M. Bowick and L. Giomi, Advances in Physics **58**, 449 (2009).
 - [12] H. S. Seung and D. R. Nelson, Physical Review A **38**, 1005 (1988).
 - [13] M. Bowick, D. Nelson, and A. Travesset, Physical Review B **62**, 8738 (2000), ISSN 0163-1829.
 - [14] J. Lidmar, L. Mirny, and D. R. Nelson, Physical Review E **68**, 051910 (2003).
 - [15] G. Vernizzi, R. Sknepnek, and M. Olvera de la Cruz, Proceedings of the National Academy of Sciences **108**, 4292 (2011).
 - [16] R. Sknepnek, G. Vernizzi, and M. Olvera de la Cruz, Soft Matter **8**, 636 (2012).
 - [17] W. Koiter, Koninklijke Nederlandse Akademie van Wetenschappen, Proceedings, Series B **69**, 1 (1966).
 - [18] M. Dias, J. Hanna, and C. Santangelo, Physical Review E **84**, 036603 (2011).
 - [19] W. Koiter, *A consistent first approximation in the general theory of thin elastic shells: Foundations and linear theory*, pt. 1 (Laboratorium voor Toegepaste Mechanica der Technische Hogeschool, 1959).
 - [20] E. Efrati, E. Sharon, and R. Kupferman, Journal of the Mechanics and Physics of Solids **57**, 762 (2009).
 - [21] M. Parrinello and A. Rahman, Journal of Applied Physics **52**, 7182 (1981).
 - [22] B. Schmidt and F. Fraternali, Journal of the Mechanics and Physics of Solids **60**, 172 (2012).
 - [23] J. Hu, T. Weigl, and R. Lipowsky, Soft Matter **7**, 6092 (2011).
 - [24] CGAL, *Computational Geometry Algorithms Library*, <http://www.cgal.org>.
 - [25] L. Jia, D. Lévy, D. Durand, M. Impérator-Clerc, A. Cao, and M. Li, Soft Matter **7**, 7395 (2011).
 - [26] X. Xing, H. Shin, M. J. Bowick, Z. Yao, L. Jia, and M.-H. Li, Proceedings of the National Academy of Sciences **109**, 5202 (2012).